J. Fluid Mech. (1967), *vol.* 29, *part* 1, *pp.* 165–175
Printed in Great Britain

Shear layers in a rotating fluid

By D. JAMES BAKER
Pierce Hall, Harvard University

(Received 19 September 1966)

A homogeneous fluid of viscosity ν is confined between two co-axial disks (vertical separation H) which rotate relative to a rotating system (angular velocity Ω). The resulting velocity field is studied for values of the parameter $\nu/2\Omega H^2$ in the range $1{\cdot}6 \times 10^{-2}$ to $1{\cdot}8 \times 10^{-3}$. The Rossby number, defined as the ratio of the relative angular velocity of the disks to the angular velocity of the system, ranged from 0·038 to 0·0041. The dependence of the resulting velocity field (interior and boundary-layer flow) on geometrical parameters, imposed surface and bottom velocities, and Ω, is in good agreement with the calculations of Stewartson and Carrier. In particular, when the two disks rotate with the same angular velocity, the width of the vertical shear layer at the edge of the disks is found to be proportional to $\Omega^{-0{\cdot}25\pm0{\cdot}02}$. When the disks rotate in opposite senses, a shear layer in the vertical velocity is observed which transports fluid from one disk to the other and whose width is proportional to $\Omega^{-0{\cdot}40\pm0{\cdot}10}$. The magnitude and shape of the observed vertical velocity is in fair agreement with a numerical integration of the theoretical results.

1. Introduction

The velocity field induced in a fluid confined between two coaxial rotating disks of finite radius and placed in a rotating system provides a simple example for both experimental and theoretical study of free shear layers. These shear layers, which occur at the edge of the disks, are physically required to effect the change in angular velocity of the main body of fluid and to balance the outflow from the boundary layer on one disk with the inflow to the boundary layer on the other. Stewartson (1957) has considered the linearized problem in detail, with the assumption $\epsilon = \nu/2\Omega H^2 \ll 1$ (ν is the viscosity of the fluid, H the vertical separation of the plates, and Ω the angular velocity of the system) and obtained formulas for the vertical and horizontal velocities in these layers. The problem separates into two parts: a symmetric case, in which the two disks rotate at the same angular velocity, and an antisymmetric case, in which the disks rotate with opposite angular velocities. In the symmetric case, a boundary layer of thickness $O([\epsilon]^{\frac{1}{4}})$ is necessary to effect the required change in the angular velocity of the main body of fluid, and a recirculation of fluid occurs, closed by a layer of thickness $O([\epsilon]^{\frac{1}{3}})$. In the antisymmetric case, no $O(1)$ change in the angular velocity of the main body of fluid is necessary. However, a shear layer in the vertical velocity occurs which transfers fluid from the Ekman layer on one disk to the Ekman layer on the other. This layer has a width $O([\epsilon]^{\frac{1}{3}})$ and the vertical velocities in it are $O([\epsilon]^{\frac{1}{3}})$.

In this paper the results of measurements which have been carried out with the above simple geometry are presented. These results verify the predictions of Stewartson. Calculations of the flow field for this particular geometry are also presented as computed by the methods of Carrier (1967). The experiments were carried out for values of the parameter $\epsilon = \nu/2\Omega H^2$ ranging from $1{\cdot}63 \times 10^{-2}$ to $1{\cdot}76 \times 10^{-3}$; the Rossby number, defined as the ratio of the relative angular velocity of the disks to the angular velocity of the system, ranged from 0·038 to 0·0041.

2. Theoretical calculations

We consider the problem of a fluid contained in a rotating system in the configuration of figure 1. The upper plate rotates with angular velocity $\Omega + \omega$, the lower plate with $\Omega \pm \omega$, where $\omega \ll \Omega$ (the plus sign denotes the 'symmetric' case,

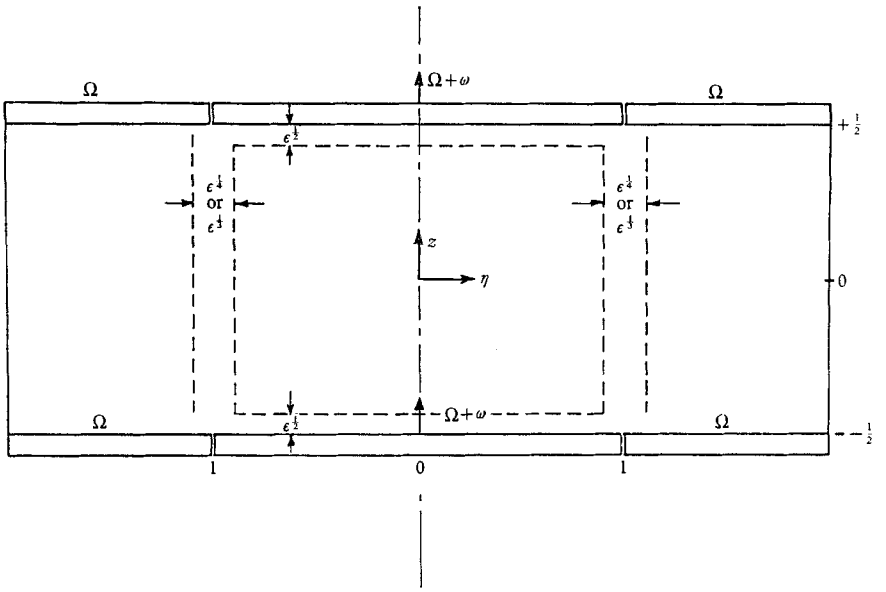

FIGURE 1. Flow configuration indicating co-ordinate system, horizontal, and vertical boundary layer regions. $\epsilon = \nu/2\Omega H^2$, where H is the separation of the plates.

the minus sign the 'antisymmetric' case). Ekman layers near $z = \pm \frac{1}{2}$ will characterize the flow in that region. However, our interest here is in the interior flow, away from these Ekman layers, and we shall consider only axially symmetric flows. All non-linear effects are ignored in this calculation. Although most of the results obtained here do not differ from those obtained by Stewartson (1957), the method of Carrier (1965, 1967) which replaces the Ekman layers by a boundary condition on the interior flow is summarized here. The reader is referred to these papers for a complete discussion of the assumptions and calculations for this type of problem. Assuming boundary-layer character for the flow, and ignoring terms to order $\epsilon^{\frac{1}{2}}$, we obtain for the governing equations of motion:

$$\left.\begin{aligned} \epsilon\Delta\Delta\psi - v_z &= 0, \\ \epsilon\Delta v + \psi_z &= 0, \end{aligned}\right\} \tag{2.1}$$

where $$\mathbf{v} = \left[-\frac{\partial \psi}{\partial z}\hat{r} + v\hat{\theta} + \frac{\partial \psi}{\partial r}\hat{z} \right],$$

and we define $$u = -\frac{\partial \psi}{\partial z}, \quad w = \frac{\partial \psi}{\partial r},$$

and we have non-dimensionalized by the vertical separation of the plates H; and velocity V_0, the appropriate V_0 to be chosen later. (A separate non-dimensionalization of r and z leads to the same results; primes denote dimensional variables.)

$$\eta = \frac{r'}{H}, \quad z = \frac{z'}{H}, \quad \psi = \psi' V_0 H, \quad v = v' V_0, \quad \epsilon = \frac{\nu}{2\Omega H^2}.$$

The boundary conditions are

$$\left.\begin{aligned} &V(\eta, +\tfrac{1}{2}) = V^+, \quad V(\eta, -\tfrac{1}{2}) = V^-, \\ &\psi(\eta, +\tfrac{1}{2}) = \psi(\eta, -\tfrac{1}{2}) = 0, \\ &\psi_z(\eta, +\tfrac{1}{2}) = \psi_z(\eta, -\tfrac{1}{2}) = 0. \end{aligned}\right\} \tag{2.2}$$

In the region far from these vertical cylindrical layers (whose width is not greater than $\epsilon^{\frac{1}{2}}$) we may describe the fluid by the following:

$$V(\eta, z) = V(\eta) + F_1(\eta, (z-\tfrac{1}{2})/\sqrt{\epsilon}) + F_2(\eta, (z+\tfrac{1}{2})/\sqrt{\epsilon}),$$
$$\psi(\eta, z) = \Phi(\eta) + G_1(\eta, (z-\tfrac{1}{2})/\sqrt{\epsilon}) + G_2(\eta, (z+\tfrac{1}{2})/\sqrt{\epsilon}).$$

To order $\sqrt{\epsilon}$, we find that the solutions F_i and G_i are of boundary-layer type; the application of the boundary conditions (2.2) implies that

$$V(\eta) = \tfrac{1}{2}[V^+(\eta) + V^-(\eta)],$$
$$\Phi(\eta) = -\tfrac{1}{2}\sqrt{(\epsilon/2)}[V^+(\eta) - V^-(\eta)].$$

Thus the interior flow is characterized by an azimuthal flow whose magnitude is the average of the imposed velocities at the upper and lower surfaces.

The boundary conditions (2.2) yield boundary conditions on the interior flow (at the edge of the Ekman layers):

$$v(-\tfrac{1}{2}, \eta) - V^-(\eta) - \sqrt{(2/\epsilon)}[\psi(-\tfrac{1}{2}, \eta)] = 0,$$

and $$v(+\tfrac{1}{2}, \eta) - V^+(\eta) + \sqrt{(2/\epsilon)}[\psi(+\tfrac{1}{2}, \eta)] = 0.$$

The velocity discontinuity at the edge of the rotating disk will be represented by the appropriate step-function: (the disks are of radius R)

$$V^{\pm} = S(x) = \left\{\begin{matrix} 1 & x > 0, \\ 0 & x < 0, \end{matrix}\right\} \quad (x = 1 - (H/R)\eta).$$

The boundary conditions then become:

$$\text{antisymmetric:} \quad v(\pm\tfrac{1}{2}, \eta) = \mp\sqrt{(2/\epsilon)}[\psi(\pm\tfrac{1}{2}, \eta] \pm S(x),$$
$$\text{symmetric:} \quad v(\pm\tfrac{1}{2}, \eta) = \mp\sqrt{(2/\epsilon)}[\psi(\pm\tfrac{1}{2}, \eta)] + S(x).$$

The use of Fourier transforms yields a convenient solution: let

$$\bar{v}(\xi, z) = \int_{-\infty}^{\infty} e^{-i\xi x} v(x, z)\, dx,$$

$$\bar{\psi}(\xi, z) = \int_{-\infty}^{\infty} e^{-i\xi x} \psi(x, z)\, dx.$$

The equations and boundary conditions imply that

$$\bar{v}^{(s)}(\xi, z) = \frac{\cosh \epsilon\xi^3 z}{i[\xi \cosh \epsilon\xi^3/2 + \sqrt{(2/\epsilon)} \sinh \epsilon\xi^3/2]},$$

$$\overline{\psi}^{(s)}(\xi, z) = \frac{-\sinh \epsilon\xi^3 z}{i\xi[\xi \cosh \epsilon\xi^3/2 + \sqrt{(2/\epsilon)} \sinh \epsilon\xi^3/2]}$$

and

$$\bar{v}^{(a)}(\xi, z) = \frac{\sinh \epsilon\xi^3 z}{i[\sqrt{(2/\epsilon)} \cosh \epsilon\xi^3/2 + \xi \sinh \epsilon\xi^3/2]},$$

$$\overline{\psi}^{(a)}(\xi, z) = \frac{\cosh \epsilon\xi^3 z}{i\xi[\sqrt{(2/\epsilon)} \cosh \epsilon\xi^3/2 + \xi \sinh \epsilon\xi^3/2]}.$$

The superscript (a) stands for antisymmetric, (s) for symmetric solution. The quantities $v^{(a)}$, $v^{(s)}$, $\psi^{(a)}$, $\psi^{(s)}$ are found by the usual inversion formula; for example,

$$v^{(a)}(x, z) = \frac{1}{2\pi} \int_{-\infty}^{\infty} \bar{v}^{(a)}(\xi, z)\, e^{i\xi x}\, d\xi.$$

All of these integrals can be evaluated as $2\pi i$ times the sum of the appropriate residues (those in the upper half plane for $x > 0$, the negative of those in the lower half plane for $x < 0$). Explicit formulas for $w^{(a)}$ and $v^{(s)}$ are obtained here for comparison with experiment. In obtaining these approximate formulas for $w^{(a)}$ and $v^{(s)}$, the fact that all the poles of the integrand lie close to either $\pm i\sqrt{2}/\epsilon$ or the roots of $\cosh(\epsilon\xi^3/2)$ or $\sinh(\epsilon\xi^3/2)$ is used. The explicit representation of these two flow fields (in this approximation) follow:

$$w^{(a)} = \frac{\epsilon^{\frac{1}{6}}\sqrt{2}}{3\pi^{\frac{2}{3}}} \sum_{n=0}^{\infty} (-1)^{n+1} \frac{\cos(2n+1)\pi z}{(2n+1)^{\frac{2}{3}}} \left[\exp\left\{-\left(\frac{2n+1}{\epsilon}\right)^{\frac{1}{3}} x\right\} + 2\exp\left\{-\frac{x}{2}\left(\frac{2n+1}{\epsilon}\right)^{\frac{1}{3}}\right\} \cos\left(\frac{\sqrt{3}}{2}\left[\frac{2n+1}{\epsilon}\pi\right]^{\frac{1}{3}} x - \tfrac{1}{3}\pi\right)\right],$$

and

$$v^{(s)} = 1 - \tfrac{1}{2}\exp\{-(2/\epsilon)^{\frac{1}{4}} x\} + \frac{\epsilon^{\frac{1}{6}}\sqrt{2}}{3\pi^{\frac{2}{3}}} \sum_{n=1}^{\infty} (-1)^{n-1} \frac{\cos(2n\pi z)}{(2n)^{\frac{2}{3}}} \left[\exp\left\{-\left(\frac{2n\pi}{\epsilon}\right)^{\frac{1}{3}} x\right\} - 2\exp\left\{-\frac{x}{2}\left(\frac{2n\pi}{\epsilon}\right)^{\frac{1}{3}}\right\} \cos\left(\frac{\sqrt{3}}{2}\left[\frac{2n\pi}{\epsilon}\right]^{\frac{1}{3}} x - \tfrac{1}{3}\pi\right)\right].$$

These formulas indicate a zonal velocity change in a layer of width $O(\epsilon^{\frac{1}{4}})$; the vertical velocity, of magnitude $\epsilon^{\frac{1}{6}}$, has a characteristic width of $\epsilon^{\frac{1}{3}}$. These formulas are valid to $O(\epsilon^{\frac{1}{3}})$; however, the measurements of vertical velocity were carried out with an ϵ such that $\epsilon^{\frac{1}{3}}$ is not negligible. In order to facilitate comparison with experiment at this ϵ, the inversion integrals were evaluated by numerical integration. The results are presented in §3.

3. Experimental results

3.1. *Experimental arrangement*

The experimental arrangement is shown in figure 2. The fluid is confined in a disk-shaped region of height 1·27 cm bounded above and below by coaxial disks of radius 12·05 cm (free to rotate relative to the rotating system) and two closely fitting outer rings (inner radius 12·05 cm, outer radius 17·14 cm) which are

stationary with respect to the rotating system. The two disks may rotate independently. The entire system is encased in an outer cylinder of lucite, and is placed on a rotating table whose axis is parallel to the axis of the disks. The use of

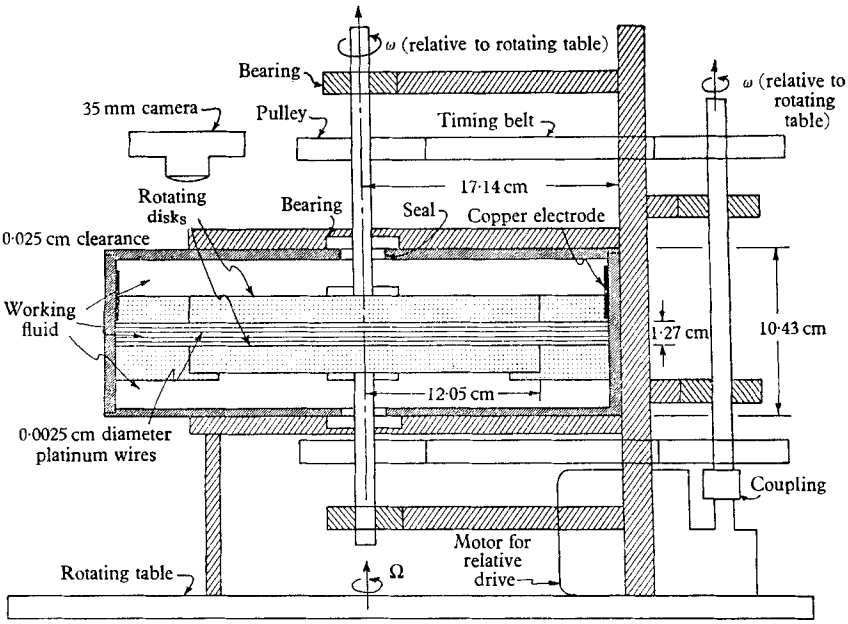

FIGURE 2. Experimental arrangement, side view (cross-section).

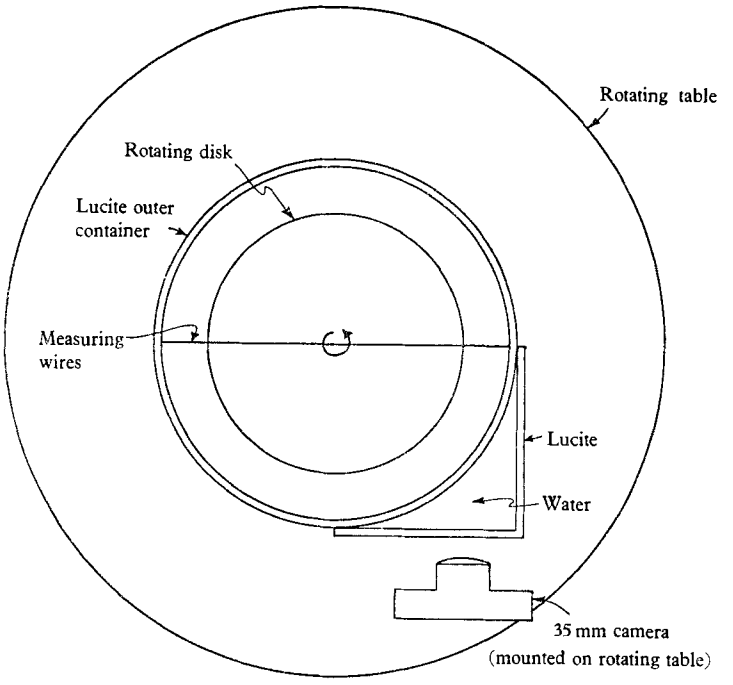

FIGURE 3. Experimental arrangement, top view.

seals near the edge of the rotating disks would preclude the study of the flow field there; a sliding fit is necessary. The whole cylinder must then be filled with fluid; the working fluid is between the disks and the outer rings. The fluid exhibited no tendency to leak out along the edges of the rotating disks. The zonal velocity structure was photographed with the camera held vertically; the vertical velocity profiles were photographed from the side through a lucite-water prism in order to minimize distortion (see figure 3).

3.2. *Measurement of velocities*

The zonal velocity change is most easily measured in the symmetric case, as the vertical shear effects an $O(1)$ change in the zonal velocity. Vertical velocities, on the other hand, are most easily measured in the antisymmetric case where the interior zonal velocity is zero (to order $\epsilon^{\frac{1}{2}}$): the undesired effects of horizontal advection of the fluid flow markers are absent. Therefore, boundary layer measurements were made of $v^{(s)}$ and $w^{(a)}$.

The validity of the above linear calculations and the avoidance of shear layer instabilities call for relative velocities of 0·1 cm/sec or smaller. These small velocities, to be measured relative to the rotating system, necessitated the development of a neutrally buoyant marker for the fluid flow.

The following method has proved successful (Baker 1966): a fine wire is placed in a solution of the pH indicator Thymol Blue which has been titrated to the end-point. A second electrode is placed in the fluid and an electric current is allowed to flow in the resulting circuit. As the pH of the solution near the wire changes, the colour of the solution there also changes; this coloured fluid will float away from the wire with the moving fluid. As the indicator is at all times in solution, the coloured fluid is precisely neutrally buoyant and thus forms a useful marker for the measurement of slow relative velocities in rotating systems.

In this particular arrangement, four 0·001 in. platinum wires were placed in the fluid as shown in figure 2. These wires are attached to the outer cylinder, thus remaining at rest relative to the rotating system. The second electrode is a copper plate around the outside of the cylinder. A current of 100 mA was necessary to obtain a line of coloured fluid sufficiently dark to photograph. All photographs were taken with a Nikon F 35 mm camera mounted on the rotating table. The system was photographed at a given time after the circuit voltage was pulsed; the resulting displacement of the coloured line of fluid is then corrected to velocity by dividing by time. (The error introduced by this averaging procedure is small compared to the other uncertainties in the experiment.) Zonal velocities were photographed 15 sec after the voltage pulse; vertical velocities 12·5 sec.

3.3. *Experimental errors*

The primary uncertainties in these measurements arise in the reduction of the data from the photographs to the actual velocity profiles. The edge of the ink profile in the enlarged photographs is not sharp; an uncertainty of 5 % is thus introduced into the velocity profile. Variations in the time between activating the dye circuit and photographing the line of dye introduced an uncertainty of 3·8 %. Other uncertainties of measurement are less than these and are neglected in

comparison. Note that the errors in the vertical velocity measurements are much larger than in the zonal velocity measurements; this difference occurs because the width of the line of dye is comparable to the distance moved by the centre of the line. An estimate of the errors due to neglect of curvature and non-linear terms in the equations of motion indicated that these terms should be less than 5 % of the terms retained.

3.4. *Experimental results*

Three different ratios of upper disk rotation rate to lower disk rotation rate were used (all measured relative to the rotating system): (*a*) the two disks had the same angular velocity, 0·0145 rad/sec; (*b*) the upper disk had an angular velocity of 0·0145 rad/sec and the lower disk did not rotate; and (*c*) the upper disk had angular velocity 0·0145 rad/sec, the lower disk $-0{\cdot}0145$ rad/sec. Case (*a*) is the 'symmetric' case, case (*b*) is mixed, and case (*c*) is 'antisymmetric'.

For each of these three arrangements, velocity measurements were carried out for values of the main rotation rate ranging over a factor of 10: from 0·38 to 3·51 rad/sec. We separate the measurements into two parts: interior flow and boundary layer (vertical shear layer) flow. (Note that for this experiment, placement of the wires precluded measurements in the Ekman layers near the upper and lower edges of the disks. The Ekman layers for these rotation rates are approximately 1 mm thick.)

Interior flow

This region is that part of the fluid between the two Ekman layers and far from the vertical shear layers. The theory predicts that the velocity in this region should be independent of z, the direction along the axis of rotation, and in each case should be the average of the imposed surface velocities. The results are depicted in table 1.

	Predicted			Observed
	V^+	V^-	$(V^+ + V^-)/2V_0$	exp V/V_0
Case (*a*)	V_0	V_0	1	$1{\cdot}03 \pm 0{\cdot}06$
Case (*b*)	V_0	0	0·5	$0{\cdot}51 \pm 0{\cdot}06$
Case (*c*)	V_0	$-V_0$	0	$0{\cdot}00 \pm 0{\cdot}06$

TABLE 1.

Excellent agreement within experimental error between the calculated and observed ratios for this interior (geostrophic) flow is exhibited here.

Boundary-layer flow

For case (*a*), the symmetric case, the zonal velocity near the edge of the disks was measured as a function of x and Ω. For the case (*c*), the antisymmetric case, the horizontal velocities are zero, and the vertical velocity profile can be measured as a function of x, z and Ω.

Photographs of the flow were obtained at nineteen different values of the main rotation rate, Ω, and a typical result is depicted in figure 4. The profile (corrected for radial variation of the interior flow) agrees within experimental error with the

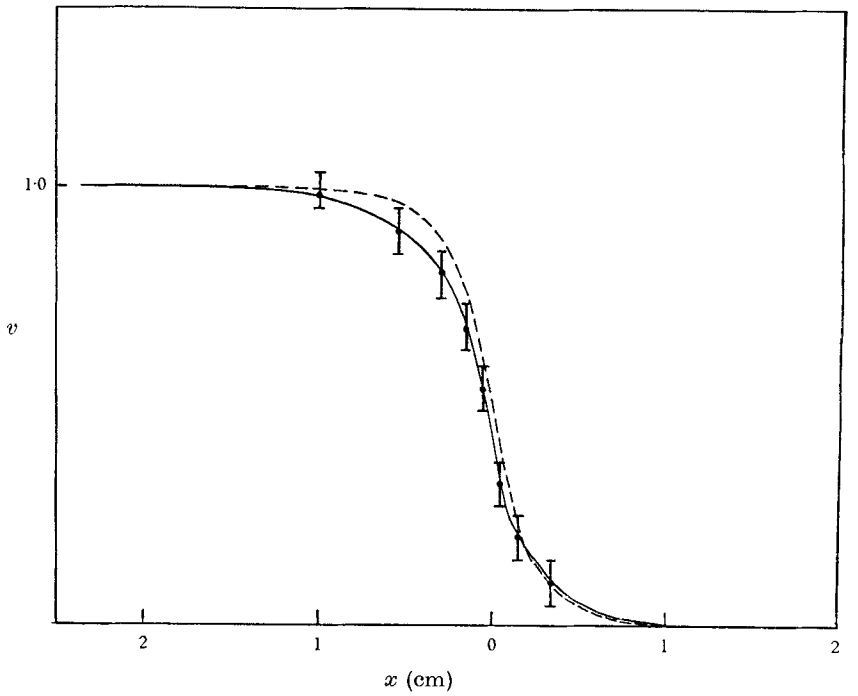

FIGURE 4. Comparison of theory and experiment for azimuthal flow near edge of disks; symmetric case. Here $\epsilon = 1{\cdot}31 \times 10^{-3}$; $\Omega = 2{\cdot}36$ sec^{-1}. Velocity non-dimensionalized by $V_0 = \omega R$; R = radius of disks. —, experiment; ---, theory; $\overline{\mathrm{I}}$, experimental uncertainty.

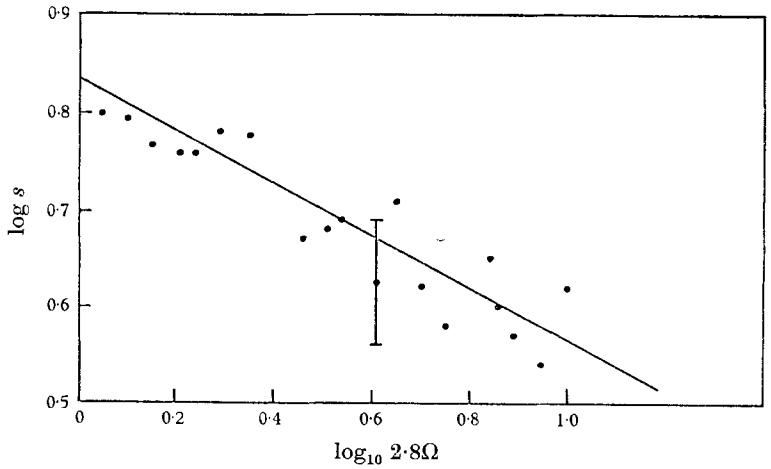

FIGURE 5. Width of azimuthal boundary layer as a function of main rotation rate Ω. Predicted slope: $-0{\cdot}25$; observed slope: $-0{\cdot}25 \pm 0{\cdot}02$. ●, experimental points; —, least squares fit to data. Slope = $-0{\cdot}25 \pm 0{\cdot}02$; $\overline{\mathrm{I}}$, typical experimental uncertainty.

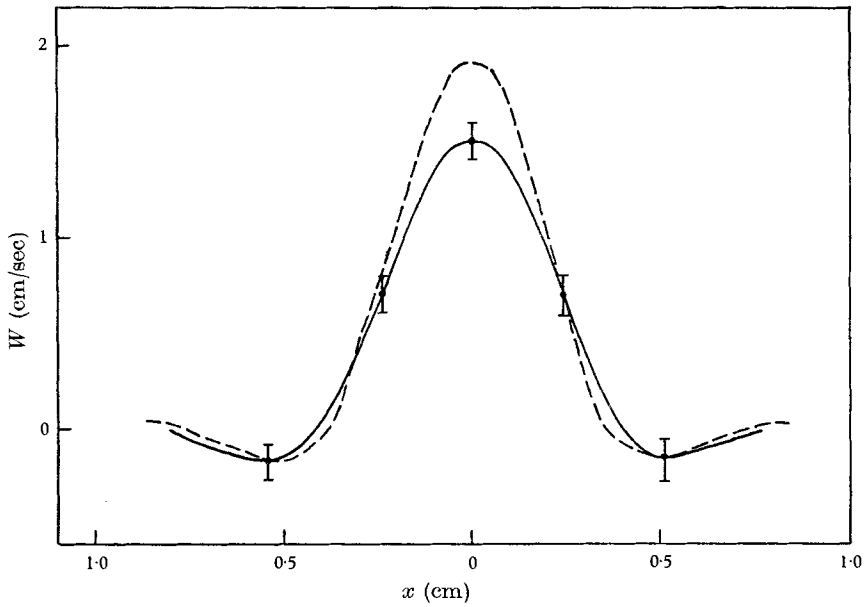

FIGURE 6. Comparison of theory and experiment for vertical velocity structure near edge of disks; antisymmetric case. Here $\epsilon = 2{\cdot}20 \times 10^{-3}$; $\Omega = 1{\cdot}41\ \text{sec}^{-1}$. —, experimental profile; ---, theory; ⊥, experimental uncertainty.

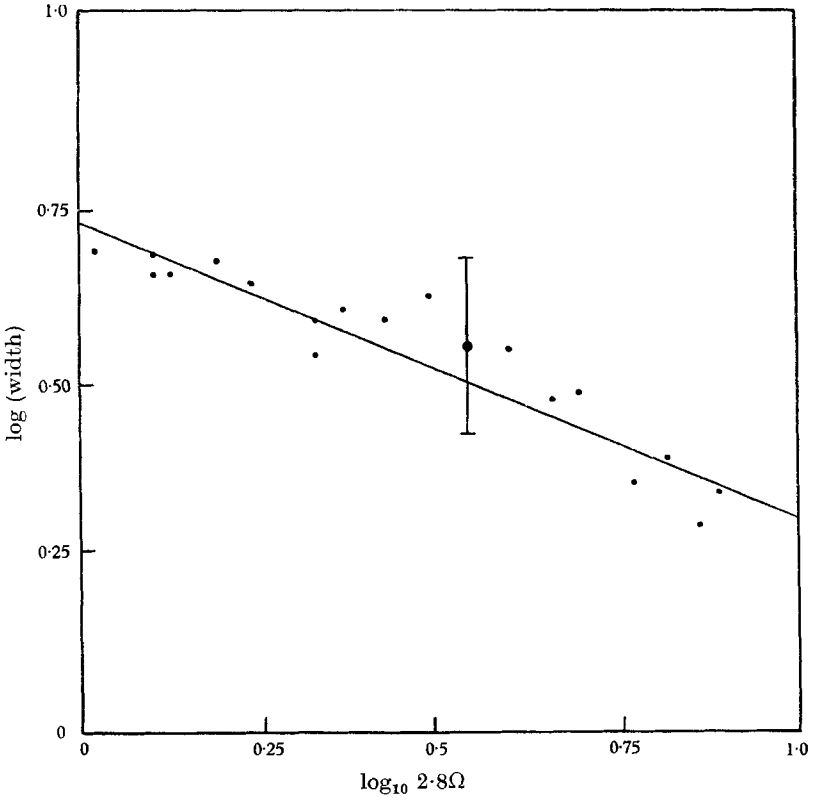

FIGURE 7. Width of vertical velocity profile as a function of main rotation rate Ω. Predicted slope $-0{\cdot}33$; observed slope $-0{\cdot}40 \pm 0{\cdot}10$. —, least squares fit line slope = $0{\cdot}40 \pm 0{\cdot}10$; ⊥, typical experimental uncertainty.

theoretical computations. In order to determine the dependence of the width of the experimental profile on the basic rotation rate, $\log v$ was plotted as a function of radius, and a least squares line was fitted to the resulting points yielding a slope S. A plot of $\log S$ against $\log \Omega$ (figure 5) yields the Ω-dependence of the profile width. A least squares fit to these points yields a slope of $-0{\cdot}25 \pm 0{\cdot}02$, which is in excellent agreement with the theoretical prediction of $-0{\cdot}25$. The $\epsilon^{\frac{1}{3}}$ structure predicted by the theory is too small in magnitude to be observable in this experiment.

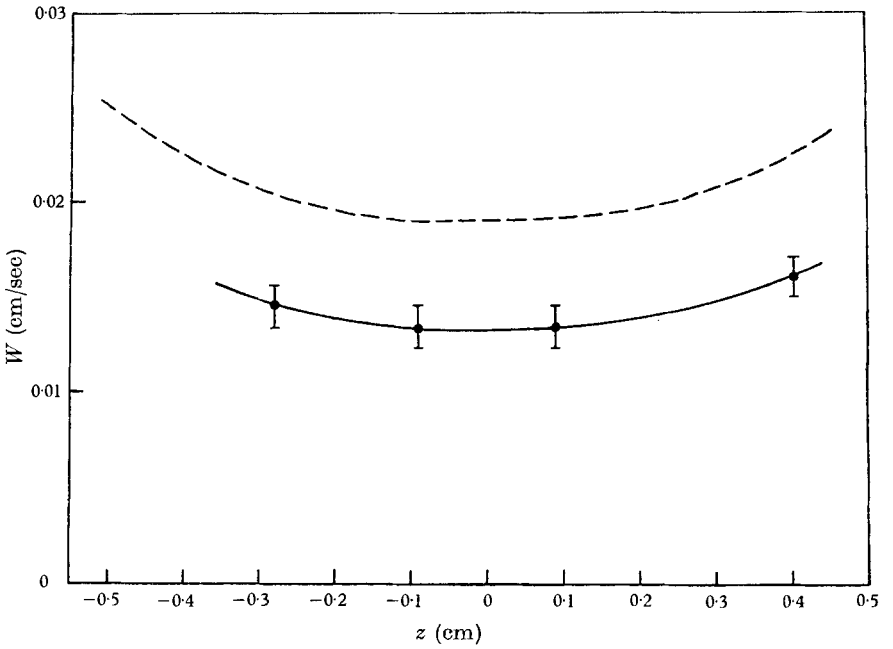

FIGURE 8. Magnitude of vertical velocity as a function of z at $x = 0$. ϵ, Ω same as figure 6. ---, theory; –•–, experimenta data; ⊤, experimental uncertainty.

A typical vertical velocity profile is depicted in figure 6. The experimental errors are somewhat larger in this case, due to the slower velocities, but the general shape of the profile is in good agreement with the theoretical profile obtained by a numerical integration of the inversion integral. This procedure was necessary in order to obtain the result correct to order $O(\epsilon^{\frac{1}{3}})$. Nineteen profiles were thus obtained. In order to determine the dependence of the width of this profile on the main rotation rate, the logarithm of the distance between the points where the velocity was zero was plotted as a function of the logarithm of the main rotation rate. The slope of the resulting line determines the Ω-dependence of the width. The result is shown in figure 7. The uncertainties are larger in this case because an average for each profile is not obtainable. However, the result $(\Omega^{-0{\cdot}40 \pm 0{\cdot}10})$ is consistent with the theoretical result of $\Omega^{-0{\cdot}33}$. As can be seen from (2.4), the vertical velocity is a slowly varying function of z. As the vertical velocity was determined at four different levels in the fluid, this z-dependence could be checked. Figure 8 depicts the theoretical results for w (at $x = 0$) as a function of z.

The four experimental points are plotted on the same graph, and the z-dependence correlates closely with the theory. The predicted magnitude of the vertical velocity is 30 % higher than the observed magnitude. This discrepancy probably lies both in the approximate treatment of the linear theory and the neglect of non-linear terms in the calculation of this small $[O(\epsilon^{\frac{1}{2}})]$ velocity. The calculations of zonal velocities yield magnitudes $O(1)$ and do not exhibit such a discrepancy. Figures 9 and 10 are actual photographs of the dye lines, exhibiting the features discussed.

It is a pleasure to acknowledge the continued interest and help of Prof. A. R. Robinson. This research was supported by a grant (NR-083-201) from the Office of Naval Research to Harvard University.

REFERENCES

BAKER, D. J. 1966. *J. Fluid Mech.* **26**, 573.

CARRIER, G. F. 1965 *J. Fluid Mech.* **23**, 145.

CARRIER, G. F. 1967 Phenomena in rotating fluids. To be published in *J. Fluid Mech.*

STEWARTSON, K. 1957 *J. Fluid Mech.* **3**, 17.

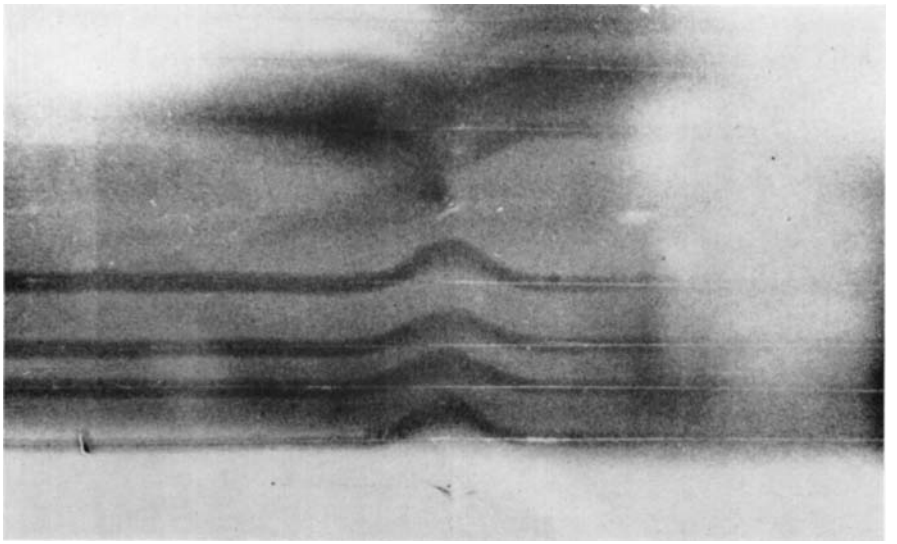

FIGURE 9. Vertical velocity in free shear layer at edge of disks; antisymmetric case. Dye lines photographed 12·5 sec after voltage pulse. Main rotation rate $\Omega = 1{\cdot}41$ sec^{-1}. The four lines in lower half of picture demonstrate actual flow; reflexions can be seen above.

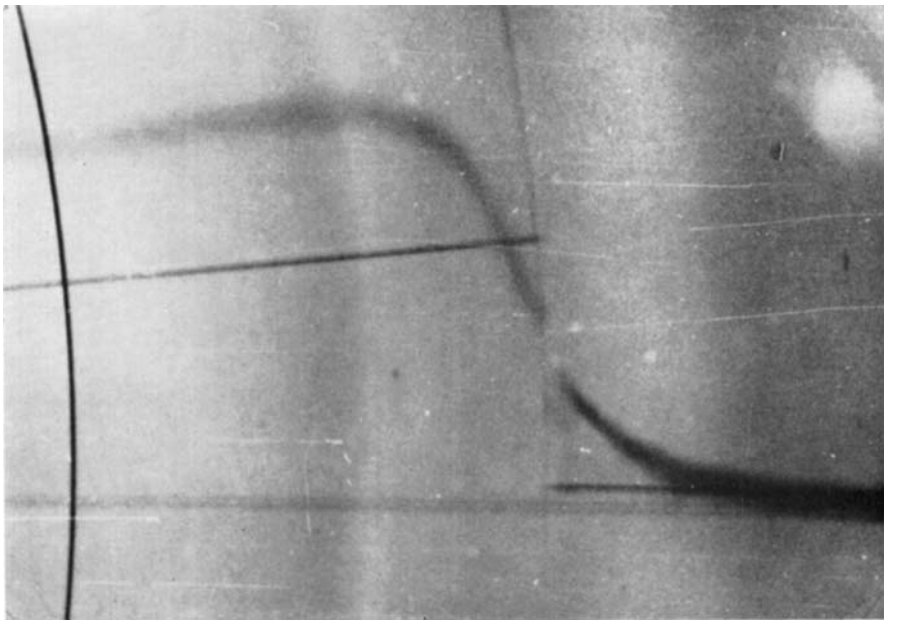

FIGURE 10. Boundary layer in azimuthal velocity at edge of disks. Dye lines photographed 15 sec after voltage pulse. Main rotation rate $\Omega = 2{\cdot}36$ sec^{-1}.